

 Open access • Posted Content • DOI:10.1101/2019.12.23.880021

## Exaptation of two ancient immune proteins into a new dimeric pore-forming toxin in snails — [Source link](#)

Matías Leonel Giglio, Santiago Ituarte, Verónica Milesi, Marcos Sebastián Dreon ...+7 more authors

**Institutions:** National Scientific and Technical Research Council, Fundación Instituto Leloir, Hong Kong Baptist University

**Published on:** 23 Dec 2019 - bioRxiv (Cold Spring Harbor Laboratory)

**Topics:** MACPF, Pore-forming toxin and AB toxin

Related papers:

- [Exaptation of two ancient immune proteins into a new dimeric pore-forming toxin in snails.](#)
- [Giant MACPF/CDC pore forming toxins: A class of their own.](#)
- [The Apicomplexan CDC/MACPF-like pore-forming proteins](#)
- [Chapter 20 – C7](#)
- [Structural basis of Toxoplasma gondii perforin-like protein 1 membrane interaction and activity during egress](#)

Share this paper:    

View more about this paper here: <https://typeset.io/papers/exaptation-of-two-ancient-immune-proteins-into-a-new-dimeric-m9jhs6jyud>

1 **Exaptation of two ancient immune proteins into a new dimeric pore-forming toxin in**  
2 **snails**

3  
4 M.L. Giglio<sup>a</sup>, S. Ituarte<sup>a</sup>, V. Milesi<sup>b</sup>, M.S. Dreon<sup>a</sup>, T.R. Broia<sup>a</sup>, J. Caramelo<sup>c</sup>, J.C.H. Ip<sup>d</sup>, S.  
5 Maté<sup>a</sup>, J.W. Qiu<sup>d</sup>, L.H. Otero<sup>c,e\*</sup> and H. Heras<sup>a\*</sup>

6  
7 a. Instituto de Investigaciones Bioquímicas de La Plata “Prof. Dr. Rodolfo R. Brenner”,  
8 INIBIOLP. CONICET CCT La Plata - Universidad Nacional de La Plata (UNLP), Facultad de  
9 Medicina, 1900 La Plata, Argentina.

10 b. Instituto de Estudios Inmunológicos y Fisiopatológicos, IIFP. CONICET CCT La Plata –  
11 UNLP, Facultad de Ciencias Exactas, 1900 La Plata, Argentina.

12 c. Instituto de Investigaciones Bioquímicas de Buenos Aires, IIBBA. CONICET- Fundación  
13 Instituto Leloir, Av. Patricias Argentinas 435, C1405BWE Buenos Aires, Argentina.

14 d. Department of Biology, Hong Kong Baptist University, 224 Waterloo Road, Hong Kong,  
15 China.

16 e. Plataforma Argentina de Biología Estructural y Metabolómica PLABEM, Av. Patricias  
17 Argentinas 435, C1405BWE, Buenos Aires, Argentina.

18  
19 **Subject Area:** Biochemistry and Chemical Biology

20 **\*Co-corresponding authors:**

21 Horacio Heras

22 Instituto de Investigaciones Bioquímicas de La Plata (INIBIOLP), Consejo Nacional de  
23 Investigaciones Científicas y Técnicas (CONICET) - Universidad Nacional de La Plata (UNLP),  
24 60 y 120, 1900 La Plata, Argentina.

25 Tel: +54 (221) 482-4894

26 Email: h-heras@med.unlp.edu.ar

27 ORCID ID: 0000-0003-3379-0216

28  
29 Lisandro H. Otero

30 Instituto de Investigaciones Bioquímicas de Buenos Aires (IIBBA), Consejo Nacional de  
31 Investigaciones Científicas y Técnicas (CONICET) - Fundación Instituto Leloir, Patricias Argentinas  
32 435, C1405BWE Buenos Aires, Argentina.

33 Tel: +054 (11) 5238-7500

34 Email: lotero@leloir.org.ar

35 ORCID ID: 0000-0002-5448-5483

37 **Abstract**

38 The Membrane Attack Complex-Perforin (MACPF) family is ubiquitously found in all  
39 kingdoms. They have diverse cellular roles but MACPF but pore-forming toxic function are  
40 very rare in animals. Here we present the structure of PmPV2, a MACPF toxin from the  
41 poisonous apple snail eggs, that can affect the digestive and nervous systems of potential  
42 predators. We report the three-dimensional structure of PmPV2, at 15 Å resolution  
43 determined by negative stain electron microscopy (NS-EM) and its solution structure by  
44 small angle X-ray scattering (SAXS). We found that PV2s differ from nearly all MACPFs in  
45 two respects: it is a dimer in solution and protomers combine two immune proteins into  
46 an AB toxin. MACPF chain is linked by a single disulfide bond to a tachylectin chain, and  
47 two heterodimers are arranged head-to-tail by non-covalent forces in the native protein.  
48 MACPF domain is fused with a putative new Ct-accessory domain exclusive to  
49 invertebrates. Tachylectin is a six-bladed  $\beta$ -propeller, similar to animal tectonins. We  
50 experimentally validated the predicted functions of both subunits and demonstrated for  
51 the first time that PV2s are true pore-forming toxins. The tachylectin "B" delivery subunit  
52 would bind to target membranes, and then its MACPF "A" toxic subunit disrupt lipid  
53 bilayers forming large pores altering the plasma membrane conductance. These results  
54 indicate that PV2s toxicity evolved by linking two immune proteins where their combined  
55 preexisting functions give rise to a new toxic entity with a novel role in defense against  
56 predation. This structure is an unparalleled example of protein exaptation.

57

58 **Keywords:** Pore-forming toxin, poisonous snail egg, PmPV2, lectin, AB toxin, *Pomacea*,  
59 chemical defense, negative stain electron microscopy, small-angle X-ray scattering

60

## 61 **Introduction**

62 The integrity of cellular membranes is crucial for life and the disruption of such integrity  
63 causes cell death. Animals have evolved many strategies for damaging membranes and  
64 pore formation by proteins is frequently used in toxic attack on cells, as it can lead to  
65 efficient disruption of cell metabolism or even cell death. Among these proteins, the  
66 largest group belongs to the Membrane Attack Complex and Perforin / Cholesterol-  
67 Dependent Cytolysins (MACPF/CDC) superfamily, with ubiquitous distribution in all  
68 kingdoms. Most characterized members of MACPF/CDC interact with membranes and  
69 form large pores (hence the name: pore-forming proteins, PFPs). MACPF proteins function  
70 in immunity and bacterial pathogenesis (Anderluh, Kisovec, Krasevec, & Gilbert, 2014) ,  
71 and a very small group, termed pore-forming toxins (PFTs), have a toxic function (Peraro &  
72 van der Goot, 2016). These PFTs are present in bacteria, protists and fungi, but are very  
73 rare in animals. In fact, MACPF PFTs were reported only in a vertebrate (stonefish) and  
74 two groups of invertebrates: Cnidaria (Anderluh et al., 2014; Ellisdon et al., 2015) and the  
75 apple snail *Pomacea canaliculata* (Dreon et al., 2013).

76 We focus on the PFTs from the poisonous eggs of *Pomacea* apple snails (Gastropoda:  
77 Ampullariidae). Among them, *Pomacea canaliculata* eggs contain the toxin perivitelin-2  
78 (PcPV2), one of the most toxic egg proteins known (Heras et al., 2008). PcPV2 is composed  
79 of two subunits, a MACPF chain, and a tachylectin-like chain [member of the F-type lectin  
80 family (Bishnoi, Khatri, Subramanian, & Ramya, 2015)], termed PcPV2-67 and PcPV2-31,  
81 respectively (Dreon et al., 2013; Heras et al., 2008). Moreover, the egg fluid (PVF) of  
82 *Pomacea maculata*, a related species, also contains a PV2-67 and PV2-31 like proteins  
83 orthologous of the two PcPV2 subunits (Mu, Sun, Heras, Chu, & Qiu, 2017).

84 PcPV2 can be included into the AB toxins, a small group of toxic proteins found in  
85 bacteria (e.g. botulinum neurotoxins) and plants (e.g. Type-2 RIP), that play a role in  
86 pathogenic processes and embryo defense, respectively. AB toxins contain two moieties,  
87 the “A” moiety that modifies some cellular target leading to cell death and the “B” moiety,  
88 which has usually a carbohydrate binding module (CBM), that recognizes glycans of the  
89 cell membrane and acts as a delivery subunit (Odumosu, Nicholas, Yano, & Langridge,

2010). Some of the CBM properties of AB toxins have been recognized in PcPV2 as it can agglutinate erythrocytes and recognize intestinal cells (Dreon et al., 2013), however, little is known about its sugar specificity and toxic mechanism. PcPV2 is unique among AB toxins in that not only the B but also the A moiety - a MACPF - has also putative membrane binding capacity, although there is no experimental confirmation of the pore-formation capacity of PV2s. For instance, experiments with mice indicate that minute quantities of PcPV2 are lethal if they enter the bloodstream (Dreon et al., 2013; Heras et al., 2008). Eggs of *P. maculata* were also poisonous and caused lethal toxicity to mice by an unidentified factor. It was observed that after PVF inoculation, severe signs pointing to nervous disorders appeared while at longer periods, mice showed paralysis of the rear limbs and even death (Giglio, Ituarte, Pasquevich, & Heras, 2016). The poisonous eggs of *P. canaliculata* and *P. maculata*, have an additional line of defense advertising the noxiousness by a bright pink coloration that warns predators (aposematic coloration) (Fig. 1A). Apple snail defensive strategy pays off and as a result eggs have very few predators (Yusa, Sugiura, & Ichinose, 2000). Here, we identified PmPV2 as the toxic factor in *P. maculata* eggs and studied its structure and putative functions. We found that PmPV2 present unique structural features compared with other MACPFs, and demonstrated that both subunits – tachylectin and MACPF – are functional, being the first experimental validation of the pore-forming capacity of PV2 toxins.

109

## 110 **Results**

### 111 ***Identification and toxic activity of PmPV2***

112 We tracked the toxin of the PVF that causes lethal toxicity in mice by protein purification  
113 (Fig. 1B) and toxicity tests. A large oligomeric protein was subsequently identified, and N-  
114 terminal sequence confirmed that the protein isolated was Perivitellin-2 (PmPV2)  
115 [Pma\_3499\_0.54 and Pma\_3499\_0.31 (Sun et al., 2019)].

116 Purified PmPV2 proved to cause the same neurological effects than previously  
117 reported for the whole *P. maculata* PVF, with a LD50,96h of 0.25 mg/Kg after i.p. injection.  
118 This pointed out that PmPV2 is responsible of the poisonous effect of snail eggs.

119

## 120 ***Structural features of PmPV2***

121 Native PmPV2 is a ~162 kDa oligomeric glycoprotein that with an anionic detergent  
122 separate into a single band of ca. 98 kDa, which upon reduction dissociates into a heavy  
123 chain (PmPV2-67) and a light chain (PmPV2-31) (Fig. 1C, D, S1). The heterodimer is joined  
124 by a single disulfide bridge between Cys161 (PmPV2-31) and Cys398 (PmPV2-67) as  
125 determined by mass spectrometry (Fig. 2A, Table S1). PmPV2-67 has two glycoforms of pI  
126 5.22 and 5.38 while PmPV2-31 has a single form (pI 8.16) as determined in two-  
127 dimensional electrophoresis (2DE) (Fig. S1).

128 Homology modeling of the two subunits allowed us to obtain structures with a  
129 reasonable match to their templates (Fig. 2B, Fig S2). Pfam analysis indicates that PmPV2-  
130 31 chain has a lectin domain that belongs to the HydWA family (PF06462, E-value=6.6e<sup>-5</sup>)  
131 (Fig. S3). This lectin-like domain was identified as structurally similar to carp fish egg lectin  
132 (4RUSD), giving a 6 bladed  $\beta$ -propeller structure model (Fig. 2B).

133 The Nt region of the PmPV2-67 chain has a MACPF domain (PF01823, E-value= 7.e<sup>-24</sup>)  
134 with the conserved signature, the Cys residues and the 3 GlyGly sites, all assumed to be  
135 important for MACPFs membrane binding (Fig. S3). The best suitable template for the  
136 MACPF module was the perforin-1 (3NSJA), an innate immune system protein. The  
137 structure modeled was a MACPF fold with their characteristic twisted and bent  $\beta$ -sheet  
138 core and its two flanking transmembrane hairpin helices (TMH1/2) of 40 and 42 residues,  
139 respectively (Fig. 2B and Fig. S3). These two helix-clusters are amphiphilic, a known  
140 requirement to unfold and insert into membranes.

141 Although both PmPV2 subunits showed low identity with their templates (Fig. S2), this  
142 is in agreement with previous reports for both lectin and MACPF families (ROSADO 2007,  
143 SLADE 2008, CHAUDI 2008, KOPEC 2013).

144 Spectroscopic measurements provided further insight into the structure, indicating  
145 that PmPV2 does not have an absorbing prosthetic group (Fig. S4A). Protein tryptophan  
146 and other aromatic amino acids are buried in a non-aqueous and highly rigid environment

147 (Fig. S4B, C). The secondary structure, with equivalent amounts of alpha helices and beta  
148 sheets (Fig. S4D and Table S2), agrees with the predicted 3D model.

149

#### 150 Negative stain reconstruction of PmPV2

151 We used negative stain electron microscopy (NS-EM) to determine the oligomeric state  
152 and obtain low-resolution structural information. Single particles of PmPV2 were perfectly  
153 distinguishable (Fig. 2C) from which a preliminary 3D map was obtained.

154 The ensuing 2D class averages (Fig. 2D) showcased a set of distinct well-defined  
155 projections revealing clear structural features. Consequently, an *ab-initio* 3D EM map of  
156 PmPV2 was obtained from reference-free 2D class averages, which was iteratively refined  
157 imposing a C2 symmetry. The final 3D map (Fig 2E) at 15.2 Å resolution according to 0.5  
158 FSC criteria (Fig. S5), showed size overall dimensions (180 Å x 95 Å), and volume (387.84  
159 Å<sup>3</sup>) consistent with a tetrameric assembly of PmPV2 subunits.

160 Despite the low-resolution, the tachylectin subunits with the typical donut-like shape  
161 (Fig 2 B,E,F), as well as the MACPF subunits with the characteristic planar structure (Fig  
162 2B,E,F), were perfectly recognizable revealing a head-to-tail quaternary rearrangement  
163 (Fig 2E).

164 Accordingly, the docking of the MACPF and tachylectin models into the EM-map,  
165 shows an antiparallel dimer-of-heterodimers assembly with a C2 symmetry (Fig. 2E). Both  
166 heterodimers are docked to each other by non-covalent forces between a tachylectin  
167 from one heterodimer and the MACPF of the other. The rest of the chain does not seem  
168 to be part of the tetramer assembly. Despite the PmPV2-67 Ct (IMAD, see below) linker  
169 domain is defined in the EM-map between the MACPF and tachylectin domains, no model  
170 information is available (Fig 2F).

171 As a whole, structural data indicate that PmPV2 can be regarded as a dimer of  
172 heterodimers held together head-to-tail by non-covalent forces, being the subunits of  
173 each heterodimer linked by a single interchain disulfide bond.

174

175 SAXS of PmPV2

176 To analyze PmPV2 overall shape and size in solution, we used small angle X-ray scattering  
177 (SAXS). Several independent *ab initio* runs yielded reproducible molecular shapes, and the  
178 average models generated are consistent with a dimeric state, in agreement with EM-NS  
179 and SEC-SLS results (Fig. 2G). SAXS analysis indicate PmPV2 has a gyration radius of  $43.9 \pm$   
180  $0.3 \text{ \AA}$  and a globular and anisometric shape (pair distance distribution  $P(r)$  with a  
181 maximum at  $43.7 \text{ \AA}$  and a  $D_{max}$  of  $142.5 \text{ \AA}$ ) compatible with a 173 kDa particle, thus both  
182 SLS and SAXS yielded similar molecular weights. The global shape of the low-resolution 3D  
183 model of PmPV2 obtained by this method is in good concordance with the NS-EM model  
184 (Fig. 2F,G).

185

#### 186 ***PmPV2 is an active lectin and is able to form transmembrane pores***

187 To analyze the activity of the tachylectin module we tested PmPV2 agglutinating capacity  
188 against rabbit red blood cells (RBC). PmPV2 above 0.8 mg/mL produced hemagglutination  
189 of intact RBC and also of those pretreated with neuraminidase (Fig. 3A). To demonstrate  
190 that the lectin activity was responsible for the agglutination, and not some other process,  
191 a control test was performed adding different sugars to inhibit agglutination. This  
192 competition assay showed that PmPV2 hemagglutinating activity was strongly inhibited by  
193 aminated monosaccharaides, while other sugars had little or no effect (Fig. 3A).

194 Considering the presence of a MACPF domain in the PmPV2-67 chain, we also  
195 evaluated the putative pore-forming activity of PV2 using Caco-2 cells, a cell line on which  
196 it binds to (Dreon et al., 2013). We examined membrane conductance changes by patch  
197 clamp techniques. Cells exposed to 29 nM PmPV2 (5  $\mu\text{g/mL}$ ) rapidly showed discrete  
198 current increments in a stepwise fashion that began to be detectable 2-3 min after the  
199 toxin was added (Fig. 3B and Fig. S6). This behavior lasted a few seconds and then the  
200 current stabilized at a final increased value respect to the control condition. From each  
201 discrete current jump, we calculated the conductance (G), obtaining a mean value of  
202  $1,116 \pm 53 \text{ pS}$  (n = 43 of six cells tested), and estimated a pore diameter ( $d$ ) of  $7.2 \text{ nm}$  ( $d =$   
203  $2\sqrt{(Gh/\sigma\pi)}$ ) assuming a solution conductivity ( $\sigma$ ) of  $1.6 \text{ S. m}^{-1}$  and a membrane thickness



204 (h) of 5 nm. This experiment showed that PmPV2 had the capacity to form pores but did  
205 not give information on whether the lectin module was needed to recognize and direct  
206 the toxin towards the membrane surface. To test this, the toxin was pre incubated with D-  
207 glucosamine before adding to the cells. After this treatment, the toxin was unable to  
208 change cell conductance, indicating that the lectin module was required for PmPV2 pore  
209 formation (Fig. 3B). This result suggested that PFT module was active and dependent on  
210 the presence of an active lectin for activity. In agreement with patch clamp results, TEM  
211 imaging of PmPV2 interaction with POPC/Cho liposomes captured pore-like structures  
212 with an inner diameter of  $5.6 \pm 0.16$  nm (Fig. 3C).

213

214 ***Phylogenetic analysis revealed a novel MACPF accessory domain exclusive of***  
215 ***invertebrates***

216 BLASTp search of PmPV2-31 chain in NCBI non-redundant database revealed 22 similar  
217 sequences, mostly belonging to lectin families. All except one, a fish egg lectin-like protein  
218 from *Rhinatrema bivittatum*, belonged to invertebrates (Fig. S7A). Remarkably, the Cys161  
219 involved in the disulfide linking of this subunit to the heavy chain, was only observed in  
220 *Pomacea* sequences (Fig. S7B). BLASTp analysis of PmPV2-67 chain showed 37 similar  
221 sequences scattered in vertebrates and invertebrates, 32 belonging to the MACPF family  
222 (Fig. S8). BLASTp searches of this sequence showed two conserved regions: an Nt-region  
223 containing the MACPF domain, and a Ct-region with a few matches with unknown  
224 proteins. A domain boundary prediction analysis by ThreaDom (Xue, Xu, Wang, & Zhang,  
225 2013) indicated that PmPV2-67 has a relatively disorganized region between the MACPF  
226 domain and the Ct-region, suggesting the subunit is composed by two different domains.  
227 Analyzing the two regions separately, residues 1-335 (Nt-PmPV2-67) and 336-565 (Ct-  
228 PmPV2-67), revealed 32 matching sequences for the Nt region, all belonging to the MACPF  
229 family of vertebrates and invertebrates. Unexpectedly, the Ct region matched 18  
230 sequences exclusive of invertebrates (Fig. 4A), 13 associated with Ct-regions of MACPF-  
231 containing proteins and 2 associated to a Notch domain (a domain involved in membrane  
232 interaction in vertebrate MACPF proteins) (Fig. 4B). Interestingly, phylogenetic analysis

233 indicates an early diversification of MACPF PmPV2 like proteins in Mollusks (Fig. 4A).  
234 Multiple sequence alignment of the Ct region with the matching sequences revealed  
235 several conserved residues, in particular many Cys (Fig. S7C). We named this novel domain  
236 "Invertebrate MACPF Accessory Domain, IMAD". Notably, *P. canaliculata* and *P. maculata*  
237 IMADs contain binding site to the tachylectin chain through a disulfide bridge, thus allowing  
238 the MACPF module attachment to the lectin. Other functions of IMAD in invertebrates  
239 remain to be investigated.

240

## 241 **Discussion**

### 242 ***PmPV2 structure and toxicity***

243 The acquisition of venoms and poisons is a transformative event in the evolution of an  
244 animal, because it remodels the predator-prey interaction from a physical to a  
245 biochemical battle, enabling animals to prey on, and defend themselves against, much  
246 larger animals (Holford, Daly, King, & Norton, 2018). Here we report the initial functional  
247 and structural characterization of PmPV2, a toxin that, according to the experimental  
248 results on mice and cell cultures, would be a potential defense of apple snail embryos  
249 against predation.

250 Although not as potent as other snail toxins such as conotoxins (Luna-Ramirez et  
251 al., 2007), PmPV2 could be consider as “highly toxic”, similar to many snake venoms  
252 (Gawade, 2004). The toxin proved lethal to mice when it entered the bloodstream and  
253 those receiving sublethal doses displayed neurological signs similar to those caused by the  
254 PVF (Giglio et al., 2016) or the PcPV2 toxin (Heras et al., 2008).

255 The general structural features of PmPV2, analyzed by spectroscopic methods and  
256 PAGE, were similar to those previously described for PcPV2 orthologous (Dreon et al.,  
257 2013; Frassa, Ceolín, Dreon, & Heras, 2010; Heras et al., 2008). Like PcPV2 (Dreon et al.,  
258 2013; Frassa et al., 2010; Heras et al., 2008), PmPV2 sequence indicate the presence of a  
259 lectin-like subunit (PmPV2-31) and a MACPF containing subunit (PmPV2-67), sharing 97 %  
260 and 96 % similarities, respectively (Mu et al., 2017). In animals, lectins and MACPFs are  
261 ubiquitous and typically related with the innate immune system (Anderluh et al., 2014;  
262 Rudd, Elliot, Cresswell, Wilson, & Dwek, 2001), the main defense system against  
263 pathogens found in invertebrates (Hoffmann, Kafatos, Janeway, & Ezenowitz, 1999). The  
264 novelty here is that in PV2s both are combined by a single disulfide bond forming lectin-  
265 MACPF heterodimers and two of these heterodimers are held together by non-covalent  
266 forces to form the native protein. Therefore, two structural features distinguish the PV2  
267 toxins from the rest of the animal PFTs: (1) they are AB toxins, with a lectin B-chain that  
268 binds to cell surface glycans and a MACPF A-chain which kills target cells by forming  
269 membrane pores; (2) unlike other MACPF, PV2s are secreted as dimers.

270 A literature search indicates that PV2s are the only reported animal toxins with a  
271 binary AB structure. Furthermore, these are the only AB toxins where the toxic moiety is a  
272 member of the MACPF family thus, instead of having toxicity by enzymatic activity to alter  
273 target cell metabolism (FALNES 2000), it affects cells by forming pores. From the  
274 functional point of view, the lectin in the AB structure would act increasing MACPF  
275 targeting specificity as compared to toxins that bind to membranes solely by protein-lipid  
276 interactions(Ros & Garcia-Saez, 2015). Remarkably, no dimeric arrangement of AB toxins  
277 was reported before.

278 In our work, SLS, SAXS and NS-EM consistently indicate that native PV2 is a dimer  
279 of heterodimers. As far as we know, there is only a single report of another MACPF  
280 secreted as a structurally-stable water-soluble dimer (Ellisdon et al., 2015) and not as  
281 monomers as the vast majority of MACPF. Interestingly, this dimeric MACPF is also a  
282 cytotoxin, the fish stonustoxin (SNTX). However, unlike PV2, SNTX do not have a lectin  
283 subunit, or even a carbohydrate-binding domain (Ellisdon et al., 2015). The reason for this  
284 dimeric arrangement is still unknown. SAXS and NS-EM derived models allowed a visual  
285 analysis of PmPV2, which reveal an antiparallel head-to-tail orientation of its protomers.  
286 In the NS-EM 3D reconstruction, the tachylectin subunit appears like a donut, which  
287 agreed with the predicted  $\beta$ -propeller structure (Bonnardel et al., 2019; Chen, Chan, &  
288 Wang, 2011; Fulop & Jones, 1999; Jawad & Paoli, 2002), whereas MACPF domain presents  
289 the characteristic flattened shape of the MACPF/CDC fold involved in oligomerization and  
290 pore formation (Rosado et al., 2007). Another interesting aspect of PmPV2 structure is the  
291 MACPF Ct domain. In vertebrates Cys-rich Ct-accessory domains are commonly located  
292 next to MACPF domains, functioning as ancillary domains key to the MACPF-membrane  
293 interaction (Peraro & van der Goot, 2016). Bioinformatic analyses of the PmPV2-67  
294 subunit revealed that in apple snails the MACPF domain is fused with a novel Ct accessory  
295 domain, which is likely enhancing its selectivity, membrane binding affinity and/or toxicity  
296 (Peraro & van der Goot, 2016; Reboul, Whisstock, & Dunstone, 2016). We found this Ct  
297 domain is conserved among many invertebrate MACPF-containing proteins, and  
298 phylogenetic analysis suggests that this combination of a MACPF and Ct-domains may

299 have been present in the last common ancestor of invertebrates. We thus propose that  
300 this conserved domain, we dubbed IMAD, is a new family of MACPF-accessory domains  
301 exclusive of invertebrates with a still unknown structure and a putative membrane  
302 recognition function. In *Pomacea*, IMAD is also the binding site to the tachylectin chain.  
303 The interaction with several membrane components to attain higher binding affinity and  
304 specificity for the target cell has been reported for other MACPF/CDC PFT (Reboul et al.,  
305 2016). This is another avenue of future research.

306

### 307 ***PmPV2 is a pore-forming toxin (PFT) delivered by a lectin***

308 The presence of a MACPF domain in the primary structure of both PcPV2 and PmPV2  
309 (DREON 2013, MU 2017), suggested a putative pore-forming activity. Here, we confirmed  
310 for the first time that PV2s are indeed PFTs and that upon binding, oligomerize into a  
311 complex that penetrate the target membrane. Patch clamp experiments also indicated  
312 that, once cells are perforated, the membrane oligomeric structures are stable. Besides,  
313 the discrete jumps in membrane conductance in a stepwise fashion is consistent with the  
314 pore-forming activity already reported for other PFTs (Marchioretto, Podobnik, Dalla  
315 Serra, & Anderluh, 2013) (Podack, Ding-E Young, & Cohn, 1986). This was further  
316 supported by the identification in the predicted structure of amphipathic sequences in the  
317 TMH1/2 together with the typical MACPF/CDC fold required to form pores. Finally, the  
318 TEM images provided a visual confirmation of pore-like structures of ~6 nm inner  
319 diameter, which agrees with the pore size estimated by patch clamp measurements, and  
320 lies within the range reported for other MACPFs (Anderluh et al., 2014).

321 We demonstrated that, beside the pore forming activity, PmPV2 is also an active  
322 lectin with a primary specificity for aminated sugars. In this regard, CBMs in other AB  
323 toxins are found to function in delivering the toxic component of the protein to cell  
324 surfaces through glycan-CBM interactions (Boraston, Lammerts van Bueren, Ficko-Blean,  
325 & Abbott, 2007). As blocking the lectin activity inhibited the pore-forming capacity on  
326 biological membranes, we could suggest that the binding of the tachylectin subunit is a

327 necessary step for the pore formation by the MACPF chain. However, further studies are  
328 needed to unveil the membrane binding and pore-formation mechanisms of this toxin.

329

### 330 ***Ecological and evolutionary implications***

331 We found that apple snail eggs have evolved a novel PFT, which, combined with other  
332 defenses of the egg, would disable essential physiological systems in prey. The toxin  
333 shows no resemblance with other gastropod toxins such as echotoxin-2 (Kawashima,  
334 Nagai, Ishida, Nagashima, & Shiomi, 2003) or conotoxins from Conidae (Olivera, Rivier,  
335 Scott, Hillyard, & Cruz, 1991; Olivera, Showers, Watkins, & Fedosov, 2014). The  
336 combination of two unrelated polypeptides resulted in a novel protein with toxic  
337 properties, a feature not concurring with the roles classically ascribed to either animal  
338 lectins or MACPFs; they have co-opted into a new PFT that would function in *Pomacea*  
339 embryo defenses against predation. This has proven successful for the snails as virtually  
340 no predator has been able to neutralize this toxin so far (Yusa et al., 2000).

341 Remarkably, co-occurrence of a MACPF and a tachylectin in non-ampullariids is  
342 restricted to an amphioxus, a reptile and a snail. However, there is no information  
343 regarding their toxicity, or whether they are covalently linked in those organisms. On the  
344 contrary, a recent genomic analysis of tachylectin and MACPF genes showed that they  
345 comprise a MACPF-tachylectin complex exclusive of the ampullariid family. This cluster  
346 went through several tandem duplications in *P. maculata*, with some copies exclusively  
347 expressed in the female albumen gland –the gland that synthesizes the egg fluid- and  
348 detected in the eggs (Sun et al., 2019). These snails have therefore evolved an optimized  
349 defense where a genetically encoded toxin that is maternally deposited in the eggs is at  
350 the same time a storage protein for the nutrition of the embryos (Heras, Garín, & Pollero,  
351 1998). Furthermore, it has been suggested that the acquisition of toxic PV2s may have  
352 enabled terrestrial egg-laying (Sun et al., 2019). A similar dual function has also been  
353 recognized in plant seeds where toxic lectins can also double as storage proteins  
354 (Lundgren, 2009).

355 In conclusion, we provide the first evidence that PV2 toxins from snail eggs are  
356 active PFTs. Apple snail PV2, however, differs in several respects from known MACPF  
357 pore-forming toxins as it is disulfide-linked to a lectin into an AB toxin arrangement and  
358 also because it is secreted as a dimer instead of a monomer in aqueous solutions. Linking  
359 two immune proteins in a new toxic entity massively accumulated in the eggs is likely to  
360 represent the key step for PV2 novel role in defense against predation, an unparalleled  
361 example of protein exaptation. To the best of our knowledge, this is the first description of  
362 an animal AB toxin directed toward cell membranes. Future work will look at whether  
363 there are differences in the pore structure and oligomerization mechanism between PV2s  
364 and other PFTs.

365

366

## 367 **Methods**

### 368 ***Eggs collection and PmPV2 purification***

369 Adult females of *Pomacea maculata* were collected in the Parana River in San Pedro  
370 (33°30'35.97" S; 59°41'52.86" W), Buenos Aires province, Argentina and kept in the  
371 laboratory (Collection permit number DI-2018-181-GDEBA-DAPYAMAGP, Government of  
372 the Buenos Aires Province). Eggs were collected within 24 h of laid and kept at -20 °C until  
373 processed. Pools of three clutches were homogenized in ice-cold 20 mM Tris-HCl, pH 7.4,  
374 keeping a 3:1 v/w buffer:sample ratio as previously described (Heras et al., 2008). The  
375 crude homogenate was sequentially centrifuged at 10,000 xg for 30 min and at 100,000 xg  
376 for 50 min to obtain the egg perivitelline fluid, PVF.

377 PmPV2 was obtained following the method described for PcPV2 (Pasquevich, Dreon, &  
378 Heras, 2014). Briefly, PVF was ultracentrifuged in a NaBr (density = 1.28 g/ml) gradient at  
379 207,000 xg for 22 h at 4 °C. Then, PmPV2 fraction was purified by high performance liquid  
380 chromatography (HPLC) using a Mono Q<sup>TM</sup> 10/100 GL (GE Healthcare Bio-Sciences AB)  
381 column using a gradient of NaCl in 20 mM Tris-HCl buffer, pH 8.5; and by size-exclusion  
382 chromatography in a Superdex 200 10/300 GL (GE Healthcare Bio-Sciences AB) column.  
383 Purity was checked by electrophoresis in 4-20 % polyacrylamide gels.

384 Protein content was determined either by the method of Lowry (Lowry, Rosenbrough,  
385 Farr, & Randall, 1951) using Bovine Serum Albumin (BSA) as standard, or using PmPV2  
386 molar extinction coefficient at 280 nm,  $\epsilon^{280nm}$  (*see below*).

387

### 388 ***Toxicity tests***

389 All studies performed with animals were carried out in accordance with the Guide for the  
390 Care and Use of Laboratory Animals (Council, 2011) and were approved by the “Comité  
391 Institucional de Cuidado y Uso de Animales de Experimentación” of the School of  
392 Medicine, UNLP (Assurance No. P08-01-2013). Animals were obtained from the  
393 Experimental Animals Laboratory of the School of Veterinary Science, UNLP. Groups of five  
394 female BALB/cAnN mice (body weight:  $16 \pm 1.1$  g) were injected intraperitoneally (i.p.)  
395 with a single dose of 200  $\mu$ L of PBS buffer (1.5 mM  $\text{NaH}_2\text{PO}_4$ , 8.1 mM  $\text{Na}_2\text{HPO}_4$ , 140 mM  
396 NaCl, 2.7 mM KCl, pH 7.4) or the same volume of a serial dilution of five concentrations of  
397 PmPV2. Median lethal dose (LD50) was determined by a lethality test 96 h after injection,  
398 statistical analysis was performed by PROBIT using EPA-Probit analysis program v1.5  
399 statistical software of the US Environmental Protection Agency (US EPA), based on  
400 Finney’s method (Finney, 1971).

401

### 402 ***Mass determination***

403 Molecular weight of native PmPV2 in solution was determined by light scattering using a  
404 Precision Detectors the column, and the chromatographic runs were performed with a  
405 buffer containing 20 mM Tris-HCl pH 7.5, 250 mM NaCl under isocratic conditions at a  
406 flow rate of 0.4 mL/min at 20 °C. The concentration of the injected sample was 1.35  
407 mg/ml. The MW of each sample was calculated relating its 90° light scattering and  
408 refractive index (RI) signals and comparison of this value with the one obtained for BSA  
409 (MW 66.5 kDa) as a standard using the software Discovery32. The reported MW values  
410 are an average between the values relating RI and UV with scattering.

411

### 412 ***Polyacrylamide gel electrophoresis (PAGE)***



413 Native and subunit composition of PmPV2 was determined by PAGE in 4-20% gradient  
414 polyacrylamide gels using Mini-Protean II System (Bio Rad Laboratories, Inc., Hercules,  
415 CA). Non-native conditions were performed using 0.1% sodium dodecyl sulfate (SDS), 0.5%  
416 dithiothreitol (DTT) and  $\beta$ -mercaptoethanol. Low and high molecular weight markers (GE  
417 Healthcare Bioscience, Uppsala, Sweden) were run in parallel. Gels were stained using  
418 Coomassie Brilliant Blue G-250. Glycosylation was detected by PAS staining following the  
419 McGuckin and McKenzie (McGuckin & McKenzie, 1958) method modified by Streitz et al  
420 (Streitz et al., 2014), using a commercial Schiff reagent (BioPack). Further analysis was  
421 performed by two-dimensional electrophoresis gels (2-DE) in an Ettan IPGphor 3 system  
422 (GE Healthcare), as previously described (Pasquevich et al., 2014) using 60  $\mu$ g of PmPV2.

423

#### 424 ***Spectroscopic analysis***

425 ***Absorbance:*** Absorption spectra of PmPV2 (0.64 mg/mL in 20 mM Tris-HCl, 150 mM NaCl  
426 buffer, pH 7.5) were recorded between 240 and 700 nm. Ten spectra of three  
427 independent pools were measured and averaged. Forth-derivative operation was applied  
428 to analyze the relative contribution of different aromatic residues (Butler, Smith, &  
429 Schenilder, 1970).

430 The molar extinction coefficient of denatured PmPV2 was experimentally determined  
431 by measuring the absorbance at 280 nm of a solution of 720  $\mu$ g of lyophilized protein in 6  
432 M guanidinium hydrochloride (GnHCl), following equation 1:

$$433 \quad C = \frac{Abs}{\epsilon} \quad [1]$$

434 where  $C$  is the protein concentration (in  $\text{mg}\cdot\text{mL}^{-1}$ ),  $Abs$  the absorbance at a given  
435 wavelength (in nm),  $\epsilon$  the molar extinction coefficient (in  $\text{mg}^{-1}\cdot\text{mL}$ ). To determine the  
436 molar extinction coefficient of the native PmPV2, the absorbance of the native and the  
437 denatured protein were measured at identical protein concentrations. Since the  
438 concentrations are equal, we combined the equation 1 of the two solutions to obtain the  
439 native molar extinction coefficient:

$$440 \quad \epsilon_{nat} = \frac{(Abs_{nat})(\epsilon_{den})}{(Abs_{den})} \quad [2]$$

441 where  $\epsilon$  is the molar extinction coefficient (in  $\text{mg}^{-1}\cdot\text{mL}$ ),  $Abs$  the absorbance at a given  
442 wavelength (in nm), subscript *nat* refers to native protein and subscript *den* refers to  
443 denatured protein.

444 All these experiments were analyzed using an Agilent 8453 UV/Vis diode array  
445 spectrophotometer (Agilent Technologies).

446

447 *Fluorescence*: Fluorescence emission spectra of PmPV2 (65  $\mu\text{g}/\text{mL}$ ) in PBS buffer were  
448 recorded in scanning mode in a Perkin-Elmer LS55 spectrofluorometer (Norwalk). Protein  
449 was excited at 280 nm (4 nm slit) and emission recorded between 275 and 437 nm.  
450 Fluorescence measurements were performed in 10 mm optical-path-length quartz-cells.  
451 The temperature was controlled at  $25\pm 1$  °C using a circulating-water bath.

452

453 *Circular dichroism*: Spectra of PmPV2 (70–140  $\mu\text{M}$ ) were recorded on a Jasco J-810  
454 spectropolarimeter using quartz cylindrical cuvettes of 1-mm or 10-mm path lengths for  
455 the far-UV (200–250 nm) and near-UV (250–310 nm) regions, respectively. Data were  
456 converted into molar ellipticity  $[\theta]_M$  ( $\text{deg}\cdot\text{cm}^2\cdot\text{dmol}^{-1}$ ) using a mean residue weight value  
457 of 115.5 g/mol for PmPV2.

458 Proportions of different secondary structures were also obtained using CD spectra  
459 in DichroWeb (Whitmore & Wallace, 2008) software using Contin and K2d algorithms.

460

461 *Small angle X-ray scattering (SAXS)*: Synchrotron SAXS data from solutions of PmPV2 in 20  
462 mM Tris, pH 7 were collected at the SAXS2 beam line at the Laboratório Nacional de Luz  
463 Síncrotron (Campina, Brazil) using MAR 165 CDD detector at a sample-detector distance of  
464 1.511 m and at a wavelength of  $\lambda = 0.155$  nm ( $I_{(s)}$  vs  $s$ , where  $s = 4\pi\sin\theta/\lambda$ , and  $2\theta$  is the  
465 scattering angle). Solute concentrations ranging between 0.8 and 2 mg/ml were measured  
466 at 20 °C. Five successive 300 second frames were collected. The data were normalized to  
467 the intensity of the transmitted beam and radially averaged; the scattering of the solvent-  
468 blank was subtracted. The low angle data collected at lower concentration were merged  
469 with the highest concentration high angle data to yield the final composite scattering

470 curve, using ATSAS 2.8.4-1 software (Konarev, Volkov, Sokolova, Koch, & Svergun, 2003).  
471 *Ab-initio* shape determination was performed using DAMIFF online ([https://www.embl-](https://www.embl-hamburg.de/biosaxs/dammif.html)  
472 [hamburg.de/biosaxs/dammif.html](https://www.embl-hamburg.de/biosaxs/dammif.html)) (Franke & Svergun, 2009) and the resulting  
473 damstart.pdb file was used to refine the model using DAMIN (Svergun, 1999) with default  
474 parameters. Raw data, fits and models were deposited in SASBDB repository (SASDEN3).  
475 (<https://www.sasbdb.org/data/SASDEN3/ohuzme8q9a/>).

476

#### 477 **Determination of disulfide bonds**

478 To identify the disulfide bond between two subunits, 10 µg of purified PmPV2 were first  
479 separated by SDS-PAGE and then visualized with colloidal Coomassie Brilliant Blue  
480 method. The 98 kDa band was sliced, alkylated with iodacetamide, and digested in-gel  
481 with mass spectrometry grade trypsin (Perkin-Elmer).

482 Peptides were desalted with Sep-Pak C18 cartridges (Waters, Milford, USA) and  
483 dried using SpeedVac concentrator (Eppendorf, Hamburg, Germany). Dried samples were  
484 reconstituted using 0.1 % formic acid for analysis using LTQ-Orbitrap Elite coupled to an  
485 Easy-nLC (Thermo Fisher, Bremen, Germany) with 80 min LC gradient: 5 min in 98%  
486 solution A (0.1% formic acid in H<sub>2</sub>O), 35 min in 7 - 20% solution B (0.1% formic acid in  
487 acetonitrile), 20 min in 20 - 35% solution B, 10 min in 35 - 90% solution B, 10 min in 90%  
488 solution B. The MS data were captured within a range of 500 to 1800 m/z. The ten most  
489 abundant multiple-charged ions with a signal threshold >500 counts were selected for  
490 fragmentation under high-energy collision-induced dissociation (HCD; 2.0 m/z of solution  
491 width 10 ms of activation time, 40% of normalized collision energy).

492 Raw data were converted to .mgf files using Proteome Discoverer 1.3.0.339  
493 (Thermo Finnigan, CA). The MS files were searched against custom proteinPmPV2  
494 databases [Pma\_3499\_0.31, Pma\_3499\_0.54 and Pma\_3499\_0.24, which were found in  
495 PmPVF (Sun et al., 2019) using the pLink-SS incorporated into pLink 2.3.5 (S. Lu et al.,  
496 2018; Shan Lu et al., 2015; Yang et al., 2012) with the cross linkage search of disulfide  
497 bond and default parameters.

498

499 ***Bioinformatic analysis***

500 PmPV2-31 and PmPV2-67 subunit sequences were annotated as Pma\_3499\_0.54 and  
501 Pma\_3499\_0.31, respectively, by Sun et al. (Sun et al., 2019). PmPV2 related-sequences  
502 from different organisms were retrieved from NCBI non-redundant database by BLASTp  
503 set as default (threshold E-value=1e-5) and aligned using MUSCLE multiple alignment tool  
504 (<https://www.ebi.ac.uk/Tools/msa/muscle/>) for homology analysis. Phylogenetic analysis  
505 was performed using MrBayes v.3.2.6 software, with four chains of 100,000 generations.  
506 The tree was sampled every 100 generations, and the final burnin value was set to 20,000.  
507 The standard deviation of the split frequencies fell below 0.05. Trees were visualized by  
508 FigTree v.1.4.3.

509 Three-dimensional structures of PmPV2 subunits were predicted by homology  
510 modeling using Phyre2 software, which applied a profile-profile alignment algorithm  
511 (Kelley, Mezulis, Yates, Wass, & Sternberg, 2015), and pdb files were visualized using UCSF  
512 Chimera 1.14 (Pettersen et al., 2004). Quality of the predicted structures was evaluated  
513 using NT-PROCHECK software. Models have a confidence level of 100 % in Phyre2, and  
514 have more than 90 % residues in the most favored and additional allowed regions in  
515 PROCHECK analysis.

516

517 **NS data acquisition of PmPV2, image processing, single-particle reconstruction, and**  
518 **refinement.**

519 PmPV2 protein samples were suspended in buffer 20 mM Tris-HCl, 150 mM NaCl, pH 8.5  
520 at 0.05 mg/ml and kept on ice before grid preparation (higher concentrations caused  
521 oligomerization of the samples on the grids). Then, 3  $\mu$ l of sample was loaded on ultrathin  
522 holey-carbon-supported grids, previously pretreated with a glow discharge system for  
523 TEM grids during 50 s, under a pressure of 37 Pa. The samples were incubated with the  
524 grids 1 min, blotted by filter papers, and then stained with uranyl acetate 2% (w/v) for 30  
525 s. The excess of stain was removed by blotting. PmPV2 EM analysis were performed at  
526 LNNano-CNPEM, Brazil (proposal ID 24346). Data acquisition was performed using a Talos  
527 F200C (Thermo Fisher) operated at 200 KV with a FEI BM-Ceta direct electron detector

528 model. Data acquisition was performed on a grid, using at a nominal magnification of  
529 73,000 X, corresponding to a calibrated pixel size of 2.02 Å per pixel and a defocus range  
530 of -2.0 to -4.0 µm. A total number of 60 micrographs were recorded with an average  
531 electron dose per image of 20 e<sup>-</sup> per Å<sup>2</sup>. Estimation of CTF, particle picking, 2D  
532 classification, reconstruction of an *ab-initio* model, and refinement were executed using  
533 the software cisTEM (Grant, Rohou, & Grigorieff, 2018). Briefly, after estimating CTF, an  
534 initial template-free particle picking was performed. The preliminary set of picked single  
535 particles (20,115 particles) was first exposed to an initial 2D classification resulting in 19  
536 classes (15,317 particles). Subsequently, 2D class averages were used for getting a  
537 preliminary *ab-initio* 3D map which was used as a reference for the refinement iterative  
538 cycles against 15,317 particles applying a C2 symmetry. The estimated average map  
539 resolution was 15.2 Å (FSC=0.5).  
540 The final EM map was sharpened with the auto sharpen tool (Terwilliger, Sobolev,  
541 Afonine, & Adams, 2018) from PHENIX (Adams et al., 2010). The models were manually  
542 adjusted as rigid bodies using UCSF CHIMERA (Pettersen et al., 2004). After fitting of the  
543 models in one half of the dimeric complex, the other half was then independently fitted  
544 into the density map. Figures were generated using UCSF-CHIMERA. The NS-EM datasets  
545 are available in the wwPDB repository (<https://deposit.wwpdb.org/deposition/>) with  
546 accession code EMD-21097.

547

#### 548 ***Lectin activity of PmPV2***

549 Rabbit blood samples were obtained from animal facilities at Universidad Nacional de La  
550 Plata by cardiac puncture and collected in sterile Alsever's solution (100 mM glucose, 20  
551 mM NaCl, and 30 mM sodium citrate, pH 7.2). Prior to use, red blood cells (RBC) were  
552 washed by centrifugation at 1,500 xg for 10 min in PBS. Hemagglutinating and hemolytic  
553 activity were assayed using a two-fold serial dilution of PmPV2 (3.4 mg/mL) as previously  
554 described (Dreon et al., 2013). Primary specificity was determined by a competition assay.  
555 Erythrocytes were incubated with PmPV2 (0.87 mg/mL) in the presence of 0.1 M of D-  
556 mannose, D-galactose, D-galactosamine, N-acetyl-D-galactosamine, D-glucose, D-

557 glucosamine, N-acetyl-D-glucosamine or D-fucose. PmPV2 concentration was selected as  
558 the concentration providing visible agglutination in previous analysis. All monosaccharides  
559 were purchased from Sigma-Aldrich.

560

#### 561 ***Microscopic analyses of PmPV2 pores***

562 *Preparation of small unilamellar vesicles (SUVs):* Multilamellar vesicles were prepared by  
563 mixing synthetic 1-palmitoyl-2-oleoyl-sn-glycero-3-phosphocholine (POPC) and cholesterol  
564 (Cho) (Avanti Polar Lipids, Birmingham, AL, USA) dissolved in HPLC-grade  
565 chloroform/methanol (3:1 molar ratio). Then samples were dried by evaporating the  
566 solvent under a stream of nitrogen and then with high vacuum for 2 h in a speed vac. The  
567 samples were hydrated in a desired volume of buffer (25 mM HEPES, 150 mM NaCl, pH  
568 7.4) with stirring to facilitate dispersion. Multilayered vesicles were sonicated in an FB-  
569 15049 sonicator bath (Fisher Scientific Inc., Waltham, MA, USA) at 30 °C for 1 h to obtain  
570 SUVs for AFM and TEM experiments.

571

572 *Transmission electron microscopy (TEM) imaging* An excess of SUVs was incubated with  
573 2.1 µM PmPV2 for 1 h at 37 °C. After treatment, 50 µL of the liposome suspension was  
574 placed onto a 300-square-mesh copper grid covered with a Formvar carbon support film  
575 (Micro to Nano VOF, Netherlands) and fixed for 1 min. Samples were then negative  
576 stained with 50 µL of a 1% (w/v) phosphotungstic acid solution for 30 s. Images at  
577 different amplifications were taken using a TEM/STEM FEI Talos F200X microscope  
578 (Thermo Scientific) at 200 keV.

579

#### 580 ***Patch-clamp recordings***

581 Caco-2 cells were allowed to settle onto the cover glass bottom of a 3 ml experimental  
582 chamber. The cells were observed with a mechanically stabilized, inverted microscope  
583 (Telaval 3, Carl Zeiss, Jena, Germany) equipped with a 40x objective lens. The chamber  
584 was perfused for 15 min, at 1 ml.min<sup>-1</sup> by gravity, with extracellular saline solution before  
585 the patch-clamp experiment was started. Application of test solutions was performed

586 through a multi barreled pipette positioned close to the cell being investigated. All  
587 experiments were performed at 22 °C. The standard tight-seal whole-cell configuration of  
588 the patch-clamp technique was used (Hamill, Marty, Neher, Sakmann, & Sigworth, 1981)  
589 following two different protocols. First, the cells were clamped using voltage ramps from -  
590 50 mV to +60 mV and the macroscopic evoked currents were measured before and after  
591 adding PmPV2 to a final concentration of 0.05 mg/mL and after washing cells with the  
592 extracellular solution. Secondly, cells were clamped at a holding potential of -50 mV,  
593 hence evoking a macroscopic holding current, which we measured before and after  
594 adding PmPV2 to a final concentration of 0.005 mg/mL to the bath solution. Glass pipettes  
595 were drawn from WPI PG52165-4 glass on a two-stage vertical micropipette puller (PP-83,  
596 Narishige Scientific Instrument Laboratories, Tokyo, Japan) and pipette resistance ranged  
597 from 2 to 4 MOhms. Ionic currents were measured with an Axopatch 200A amplifier (Axon  
598 Instruments, Foster City, CA) filtered at 2 kHz, and digitized (Digidata 1440 Axon  
599 Instruments, Foster City, CA) at a sample frequency of 20 kHz. The extracellular saline  
600 solution used for recording whole cell ionic currents had a composition similar to the  
601 physiological extracellular solution containing 130 mM NaCl, 4.7 mM KCl, 2.5 mM CaCl<sub>2</sub>, 6  
602 mM glucose, and 5 mM HEPES; the intracellular solution had 130 mM KCl, 5 mM Na<sub>2</sub>ATP,  
603 1 mM MgCl<sub>2</sub>, 0.1 mM EGTA, and 5 mM HEPES. The pH of both solutions was adjusted to  
604 7.4 and 7.2, respectively, with NaOH

605

#### 606 ***Accession numbers***

607 The NS-EM density map has been deposited in the EMBD under accession code EMD-  
608 21097. The SAXS data has been deposited in the SASBDB under accession code SASDEN3.

609

#### 610 **Availability of data and material**

611 The datasets generated during the SAXS experiments are available in the SASBDB  
612 repository (<https://www.sasbdb.org/data/SASDEN3/ohuzme8q9a/>). The NS-EM datasets  
613 are available in the wwPDB repository (<https://deposit.wwpdb.org/deposition/>) with

614 accession code EMD-21097. All other data generated or analysed during this study are  
615 included in this published article and its supplementary information files.

616

## 617 **Acknowledgements**

618 SI, LHO, JC, VM and HH are members of CONICET, Argentina. MSD is member of CIC.BA,  
619 Argentina. TB and MLG are Doctoral and Postdoctoral students, respectively with  
620 scholarships from CONICET. We thank L. Bauzá for her technical assistance. We are  
621 grateful to Single Particle Cryo-EM staff from Brazilian Nanotechnology National  
622 Laboratory (LNNano, Campinas) for providing access to their facilities and for the technical  
623 assistance during EM experiments. We thank LNLS - Brazilian Synchrotron Light Laboratory  
624 for access to their facilities and for the technical assistance during SAXS experiments.

625

## 626 **Competing interests**

627 We have no competing interests.

628

## 629 **References**

- 630 Adams, P. D., Afonine, P. V., Bunkoczi, G., Chen, V. B., Davis, I. W., Echols, N., . . . Zwart, P. H.  
631 (2010). PHENIX: a comprehensive Python-based system for macromolecular structure  
632 solution. *Acta Crystallogr D Biol Crystallogr*, *66*(Pt 2), 213-221.  
633 doi:10.1107/S0907444909052925
- 634 Anderluh, G., Kisovec, M., Krasevec, N., & Gilbert, R. J. (2014). Distribution of MACPF/CDC  
635 proteins. *Subcell. Biochem*, *80*, 7-30. doi:10.1007/978-94-017-8881-6\_2 [doi]
- 636 Bishnoi, R., Khatri, I., Subramanian, S., & Ramya, T. N. (2015). Prevalence of the F-type lectin  
637 domain. *Glycobiology*, *25*(8), 888-901. doi:10.1093/glycob/cwv029
- 638 Bonnardel, F., Kumar, A., Wimmerova, M., Lahmann, M., Perez, S., Varrot, A., . . . Imberty, A.  
639 (2019). Architecture and Evolution of Blade Assembly in beta-propeller Lectins. *Structure*,  
640 *27*(5), 764-775 e763. doi:10.1016/j.str.2019.02.002
- 641 Boraston, A. B., Lammerts van Bueren, A., Ficko-Blean, E., & Abbott, D. W. (2007). Chapter 3.29.  
642 Carbohydrate-Protein Interactions: Carbohydrate-Binding Modules. In J. P. Kamerling (Ed.),  
643 *Comprehensive Glycoscience. From Chemistry to Systems Biology Vol 3* (pp. 661-696).  
644 Utrecht: Elsevier Science. (Reprinted from: In File).
- 645 Butler, W., Smith, J. C. P., & Schenilider, H. (1970). Analysis of fourth derivative spectra. *Biochim.*  
646 *Biophys. Acta*, *12*, 451-456. doi:10.1111/j.1751-1097.1970.tb06077.x
- 647 Chen, C. K., Chan, N. L., & Wang, A. H. (2011). The many blades of the beta-propeller proteins:  
648 conserved but versatile. *Trends Biochem Sci*, *36*(10), 553-561.  
649 doi:10.1016/j.tibs.2011.07.004



- 650 Council, N. R. (2011). *Guide for the Care and Use of Laboratory Animals* (8th ed.). Washington, DC:  
651 National Academies Press.
- 652 Dreon, M. S., Frassa, M. V., Ceolin, M., Ituarte, S., Qiu, J. W., Sun, J., . . . Heras, H. (2013). Novel  
653 animal defenses against predation: A snail egg neurotoxin combining lectin and pore-  
654 forming chains that resembles plant defense and bacteria attack toxins. *PLoS One*, *8*(5),  
655 e63782. doi:10.1371/journal.pone.0063782
- 656 Ellisdon, A. M., Reboul, C. F., Panjekar, S., Huynh, K., Oellig, C. A., Winter, K. L., . . . McGowan, S.  
657 (2015). Stonefish toxin defines an ancient branch of the perforin-like superfamily. *Proc*  
658 *Natl Acad Sci U S A*, *112*(50), 15360-15365. doi:10.1073/pnas.1507622112
- 659 Finney, D. J. (1971). *Probit Analysis* (3rd ed.). New York: Cambridge University Press.
- 660 Franke, D., & Svergun, D. I. (2009). DAMMIF, a program for rapid ab-initio shape determination in  
661 small-angle scattering. *Journal of Applied Crystallography*, *42*(2), 342-346.  
662 doi:10.1107/S0021889809000338
- 663 Frassa, M. V., Ceolin, M., Dreon, M. S., & Heras, H. (2010). Structure and stability of the neurotoxin  
664 PV2 from the eggs of the Apple Snail *Pomacea canaliculata*. *Biochim. Biophys. Acta*, *1804*,  
665 1492-1499. doi:10.1016/j.bbapap.2010.02.013
- 666 Fulop, V., & Jones, D. T. (1999). Beta propellers: structural rigidity and functional diversity. *Curr*  
667 *Opin Struct Biol*, *9*(6), 715-721. Retrieved from  
668 <http://www.ncbi.nlm.nih.gov/pubmed/10607670>
- 669 Gawade, S. P. (2004). Snake venom neurotoxins: Pharmacological classification. *J. toxicol. Toxin*  
670 *reviews*, *23*(1), 37-96.
- 671 Giglio, M. L., Ituarte, S., Pasquevich, M. Y., & Heras, H. (2016). The eggs of the apple snail *Pomacea*  
672 *maculata* are defended by indigestible polysaccharides and toxic proteins. *Can. J. Zool.*,  
673 *94*(11), 777-785. doi:10.1139/cjz-2016-0049
- 674 Grant, T., Rohou, A., & Grigorieff, N. (2018). cisTEM, user-friendly software for single-particle  
675 image processing. *Elife*, *7*. doi:10.7554/eLife.35383
- 676 Hamill, O. P., Marty, A., Neher, E., Sakmann, B., & Sigworth, F. J. (1981). Improved patch-clamp  
677 techniques for high-resolution current recording from cells and cell-free membrane  
678 patches. *Pflugers Arch*, *391*(2), 85-100.
- 679 Heras, H., Frassa, M. V., Fernández, P. E., Galosi, C. M., Gimeno, E. J., & Dreon, M. S. (2008). First  
680 egg protein with a neurotoxic effect on mice. *Toxicon*, *52*, 481-488.  
681 doi:10.1016/j.toxicon.2008.06.022
- 682 Heras, H., Garín, C. F., & Pollero, R. J. (1998). Biochemical composition and energy sources during  
683 embryo development and in early juveniles of the snail *Pomacea canaliculata* (Mollusca:  
684 Gastropoda). *Journal of Experimental Zoology*, *280*, 375-383. doi:10.1002/(SICI)1097-  
685 010X(19980415)280:6<375::AID-JEZ1>3.0.CO;2-K
- 686 Hoffmann, J. A., Kafatos, F. C., Janeway, J., C.A. & Ezenowitz, R. A. B. (1999). Phylogenetic  
687 perspectives in innate immunity. *Science*, *284*, 1313-1318.
- 688 Holford, M., Daly, M., King, G. F., & Norton, R. S. (2018). Venoms to the rescue. *Science*, *361*(6405),  
689 842-844. doi:10.1126/science.aau7761
- 690 Jawad, Z., & Paoli, M. (2002). Novel Sequences Propel Familiar Folds. *Structure*, *10*(4), 447-454.  
691 doi:10.1016/s0969-2126(02)00750-5
- 692 Kawashima, Y., Nagai, H., Ishida, M., Nagashima, Y., & Shiomi, K. (2003). Primary structure of  
693 echotoxin 2, an actinoporin-like hemolytic toxin from the salivary gland of the marine  
694 gastropod *Monoplex echo*. *Toxicon*, *42*(5), 491-497.
- 695 Kelley, L. A., Mezulis, S., Yates, C. M., Wass, M. N., & Sternberg, M. J. E. (2015). The Phyre2 web  
696 portal for protein modeling, prediction and analysis. *Nature Protocols*, *10*, 845.  
697 doi:10.1038/nprot.2015.053

- 698 Konarev, P. V., Volkov, V. V., Sokolova, A. V., Koch, M. H. J., & Svergun, D. I. (2003). PRIMUS: a  
699 Windows PC-based system for small-angle scattering data analysis. *Journal of Applied*  
700 *Crystallography*, 36(5), 1277-1282. doi:10.1107/s0021889803012779
- 701 Lowry, O. H., Rosenbrough, N. J., Farr, A. L., & Randall, R. (1951). Protein measurement with the  
702 Folin phenol reagent. *J. Biol. Chem.*, 193, 265-275.
- 703 Lu, S., Cao, Y., Fan, S. B., Chen, Z. L., Fang, R. Q., He, S. M., & Dong, M. Q. (2018). Mapping disulfide  
704 bonds from sub-micrograms of purified proteins or micrograms of complex protein  
705 mixtures. *Biophys Rep*, 4(2), 68-81. doi:10.1007/s41048-018-0050-6
- 706 Lu, S., Fan, S.-B., Yang, B., Li, Y.-X., Meng, J.-M., Wu, L., . . . Dong, M.-Q. (2015). Mapping native  
707 disulfide bonds at a proteome scale. *Nature Methods*, 12, 329. doi:10.1038/nmeth.3283
- 708 Luna-Ramirez, K. S., Aguilar, M. B., Falcon, A., Heimer de la Cotera, E. P., Olivera, B. M., & Maillo,  
709 M. (2007). An O-conotoxin from the vermivorous *Conus spurius* active on mice and  
710 mollusks. *Peptides*, 28(1), 24-30. doi:10.1016/j.peptides.2006.08.025
- 711 Lundgren, J. G. (2009). Seed Nutrition and Defense *Relationships of Natural Enemies and Non-Prey*  
712 *Foods* (7 ed., pp. 183-209): Springer Netherlands. (Reprinted from: Not in File).
- 713 Marchioretto, M., Podobnik, M., Dalla Serra, M., & Anderluh, G. (2013). What planar lipid  
714 membranes tell us about the pore-forming activity of cholesterol-dependent cytolysins.  
715 *Biophys Chem*, 182, 64-70. doi:10.1016/j.bpc.2013.06.015
- 716 McGuckin, W. F., & McKenzie, B. F. (1958). An improved periodic acid fuchsin sulfite staining  
717 method for evaluation of glycoproteins. *Clin. Chim*, 4(6), 476-479.
- 718 Mu, H., Sun, J., Heras, H., Chu, K. H., & Qiu, J. W. (2017). An integrated proteomic and  
719 transcriptomic analysis of perivitelline fluid proteins in a freshwater gastropod laying aerial  
720 eggs. *J. Proteomics*, 155, 22-30. doi:10.1016/j.jprot.2017.01.006
- 721 Odumosu, O., Nicholas, D., Yano, H., & Langridge, W. (2010). AB Toxins: A Paradigm Switch from  
722 Deadly to Desirable. *Toxins. (Basel)*, 2(7), 1612-1645. doi:10.3390/toxins2071612  
723 [doi];toxins-02-01612 [pii]
- 724 Olivera, B. M., Rivier, J., Scott, J. K., Hillyard, D. R., & Cruz, L. J. (1991). Conotoxins. *J. Biol. Chem*,  
725 266(33), 22067-22070.
- 726 Olivera, B. M., Showers, C. P., Watkins, M., & Fedosov, A. (2014). Biodiversity of cone snails and  
727 other venomous marine gastropods: evolutionary success through neuropharmacology.  
728 *Annu. Rev. Anim Biosci*, 2, 487-513. doi:10.1146/annurev-animal-022513-114124 [doi]
- 729 Pasquevich, M. Y., Dreon, M. S., & Heras, H. (2014). The major egg reserve protein from the  
730 invasive apple snail *Pomacea maculata* is a complex carotenoprotein related to those of  
731 *Pomacea canaliculata* and *Pomacea scalaris*. *Comp. Biochem. Physiol.*, 169 B, 63-71.  
732 doi:10.1016/j.cbpb.2013.11.008
- 733 Peraro, M. D., & van der Goot, F. G. (2016). Pore-forming toxins: ancient, but never really out of  
734 fashion. *Nat Rev Microbiol*, 14(2), 77-92. doi:10.1038/nrmicro.2015.3
- 735 Pettersen, E. F., Goddard, T. D., Huang, C. C., Couch, G. S., Greenblatt, D. M., Meng, E. C., & Ferrin,  
736 T. E. (2004). UCSF Chimera--a visualization system for exploratory research and analysis. *J*  
737 *Comput Chem*, 25(13), 1605-1612. doi:10.1002/jcc.20084
- 738 Podack, E. R., Ding-E Young, J., & Cohn, A. (1986). Isolation and biochemical and functional  
739 characterization of perforin 1 from cytolytic T-cell granules. *Proc Natl Acad Sci U S A*, 83(9),  
740 3050-3050.
- 741 Reboul, C. F., Whisstock, J. C., & Dunstone, M. A. (2016). Giant MACPF/CDC pore forming toxins: A  
742 class of their own. *Biochim Biophys Acta*, 1858(3), 475-486.  
743 doi:10.1016/j.bbamem.2015.11.017
- 744 Ros, U., & Garcia-Saez, A. J. (2015). More Than a Pore: The Interplay of Pore-Forming Proteins and  
745 Lipid Membranes. *J Membr Biol*, 248(3), 545-561. doi:10.1007/s00232-015-9820-y

- 746 Rosado, C. J., Buckle, A. M., Law, R. H., Butcher, R. E., Kan, W. T., Bird, C. H., . . . Whisstock, J. C.  
747 (2007). A common fold mediates vertebrate defense and bacterial attack. *Science*,  
748 317(5844), 1548-1551. doi:1144706 [pii];10.1126/science.1144706 [doi]
- 749 Rudd, P. M., Elliot, T., Cresswell, P., Wilson, I. A., & Dwek, R. A. (2001). Glycosylation and the  
750 immune system. *Science*, 291, 2370-2376.
- 751 Streitz, J. M., Madden, M. T., Salo, W., Bernadino, K. P., Deutsch, J. L., & Deutsch, J. C. (2014).  
752 Differentiation of mucinous from non-mucinous pancreatic cyst fluid using dual-stained, 1  
753 dimensional polyacrylamide gel electrophoresis. *Clin Proteomics*, 11(1), 42.  
754 doi:10.1186/1559-0275-11-42
- 755 Sun, J., Mu, H., Ip, J. C. H., Li, R., Xu, T., Accorsi, A., . . . Qiu, J. W. (2019). Signatures of Divergence,  
756 Invasiveness and Terrestrialization Revealed by Four Apple Snail Genomes. *Mol Biol Evol*,  
757 36(1), 1507-1520. doi:10.1093/molbev/msz084
- 758 Svergun, D. I. (1999). Restoring low resolution structure of biological macromolecules from  
759 solution scattering using simulated annealing. *Biophys. J*, 76(6), 2879-2886.
- 760 Terwilliger, T. C., Sobolev, O. V., Afonine, P. V., & Adams, P. D. (2018). Automated map sharpening  
761 by maximization of detail and connectivity. *Acta Crystallogr D Struct Biol*, 74(Pt 6), 545-  
762 559. doi:10.1107/S2059798318004655
- 763 Whitmore, L., & Wallace, B. A. (2008). Protein secondary structure analyses from circular  
764 dichroism spectroscopy: methods and reference databases. *Biopolymers*, 89(5), 392-400.  
765 doi:10.1002/bip.20853
- 766 Xue, Z., Xu, D., Wang, Y., & Zhang, Y. (2013). ThreaDom: extracting protein domain boundary  
767 information from multiple threading alignments. *Bioinformatics*, 29(13), i247-256.  
768 doi:10.1093/bioinformatics/btt209
- 769 Yang, B., Wu, Y.-J., Zhu, M., Fan, S.-B., Lin, J., Zhang, K., . . . Dong, M.-Q. (2012). Identification of  
770 cross-linked peptides from complex samples. *Nature Methods*, 9, 904.  
771 doi:10.1038/nmeth.2099
- 772 Yusa, Y., Sugiura, N., & Ichinose, K. (2000). Predation on the apple snail, *Pomacea canaliculata*  
773 (*Ampullariidae*), by the Norway rat, *Rattus norvegicus*, in the field. *Veliger*, 43(4), 349-353.

774

775 **Declarations**

776 *Ethics approval and consent to participate*

777 The experiment with mice was approved by the “Comité Institucional para el Cuidado y  
778 Uso de Animales de Laboratorio” (CICUAL) of the School of Medicine, Universidad  
779 Nacional de La Plata (UNLP) (Assurance No. P 01012016) and were carried out in  
780 accordance with the Guide for the Care and Use of Laboratory Animals (Guide for care and  
781 use of laboratory animals. Washington: Academic Press; 2011).

782

783 *Authors' contributions*

784 SI MG MSD SM VM HH conceived and designed the experiments. MG SI JC SM TB VM MSD  
785 JI LHO performed the experiments. MG JI JWQ MSD SI VM SB EP JC LHO HH analysed the  
786 data. HH JWQ JC VM LHO contributed reagents/materials/analysis tools. MG SI MSD JC SM  
787 TB LHO VM JWQ JI HH wrote the paper.

788

789 **Funding**

790 This work was supported by funding from Ministry of Science and Technology of Argentina  
791 Grant (Agencia Nacional de Promoción Científica y Tecnológica, PICT 2014-0850 to HH and  
792 PICT 2013-0122 to SI.), Consejo Nacional de Investigaciones Científicas y Técnicas,  
793 CONICET (PIP 0051 to HH), General Research Fund of Hong Kong (HKBU 12301415 to JW  
794 Q), and by partial financial support from LNLS–Brazilian Synchrotron Light Laboratory/MCT  
795 (Project SAXS1-17746), and LNNano (Project TEM 24346).

bioRxiv preprint doi: <https://doi.org/10.1101/2019.12.23.880021>; this version posted December 23, 2019. The copyright holder for this preprint (which was not certified by peer review) is the author/funder, who has granted bioRxiv a license to display the preprint in perpetuity. It is made available under aCC-BY-ND 4.0 International license.

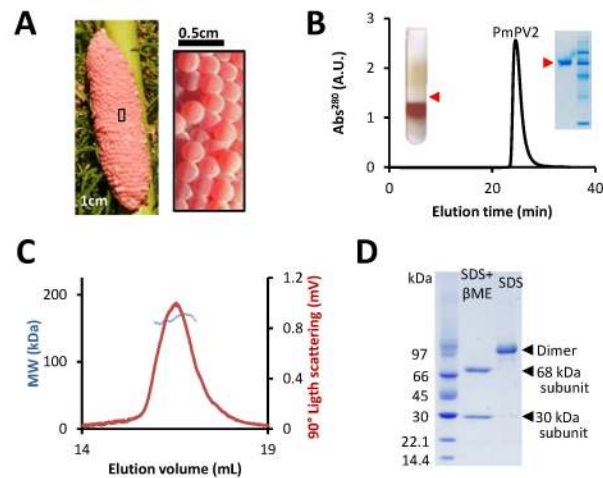


**Figure 1. Identification of PV2 toxin from the poisonous eggs of *P. maculata*.**

(A) Egg clutch of the apple snail *P. maculata*. (B) Egg fluid from apple snail eggs was subjected to ultracentrifugation in NaBr gradient and isolation of native PmPV2 by ionic exchange and exclusion columns. *Insets*: ultracentrifugation tube showing PVF fractions and native-PAGE of purified PmPV2 (red arrowheads). (C) PmPV2 toxicity: Lethality of mice recorded after i.p. injection of PmPV2 and then fitted to a Hill equation (5 animals per group) (a); Cytotoxic effect on Caco-2 cells evaluated using MTT assay (b). (D) Molecular mass determination PmPV2 by SLS. (E) PmPV2 subunit composition analyzed by SDS-PAGE demonstrates the sample is dimeric with a single band corresponding to dimeric PmPV2 shown in lane SDS. Lane SDS+  $\beta$ ME shows a sample that has been deliberately monomerized following incubation with  $\beta$ -mercaptoethanol ( $\beta$ ME) as reducing agent.



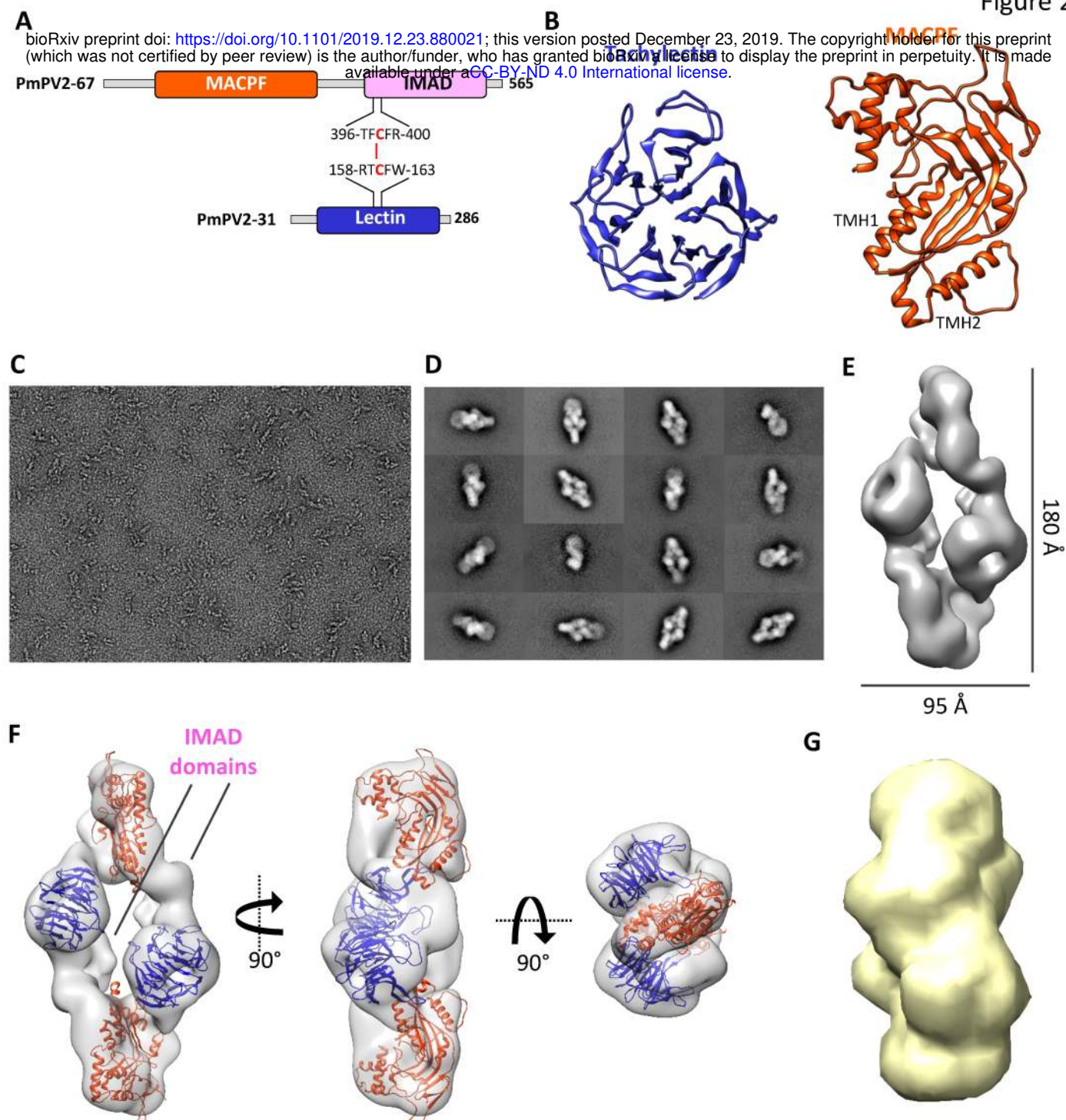


**Figure 2. Tertiary and quaternary structure of PmPV2.** (A) Schematic architecture of PmPV2. Domains are shown in orange (MACPF), purple (IMAD) and blue (Lectin) boxes. The cysteine residues involved in the interchain disulfide bond are highlighted in red. (B) 3D homology modeling of PmPV2 subunits highlighting characteristic regions of 6-blade  $\beta$ -propeller lectin domain in PmPV2-31 subunit (left), and MACPF domain in PmPV2-67 (right). (C) Representative EM-NS micrograph of PmPV2. (D) Gallery of representative 2D class averages showing the most populated views of the protein. (E) 3D EM map of PmPV2 obtained from reference-free 2D class averages. The monomers (A and B) form AB dimers, which further assemble in a “head-to-tail configuration” fashion as a tetramer. Scale bars are displayed. Rigid-body fitting of MACPF (orange) and Lectin (blue) domains into the NS-EM density map (transparent gray). Different orientation are shown to illustrate the fitted domains across the dimer-of-heterodimers. The models were rigidly docked into the map using UCSF-Chimera. (G) PmPV2 *ab-initio* volume obtained by SAXS (yellow).

bioRxiv preprint doi: <https://doi.org/10.1101/2019.12.23.880021>; this version posted December 23, 2019. The copyright holder for this preprint (which was not certified by peer review) is the author/funder, who has granted bioRxiv a license to display the preprint in perpetuity. It is made available under aCC-BY-ND 4.0 International license.

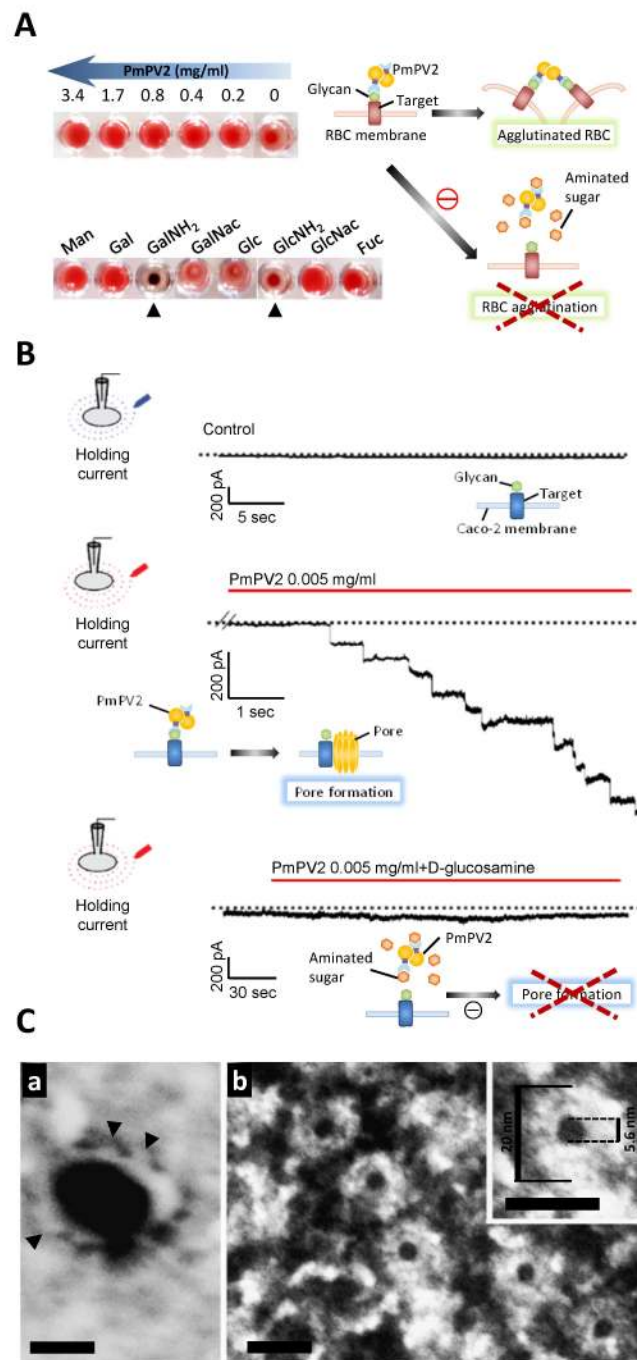


**Figure 3. PmPV2 form pores and perforates membranes.**

(A) Lectin activity of PmPV2 on erythrocytes (upper panel) and hemagglutinating activity of PmPV2 preincubated with monosaccharides (lower panel). D-mannose (Man), D-galactose (Gal), D-galactosamine (GalNH<sub>2</sub>), N-acetyl-D-galactosamine (GalNac), D-glucose (Glc), D-glucosamine (GlcNH<sub>2</sub>), N-acetyl-D-glucosamine (GlcNac), L-Fucose (Fuc). (B) Patch clamp experiments: Typical whole cell holding current obtained from a Caco-2 cell continuously clamped at -50 mV, before (upper panel) and after extracellular perfusion of PmPV2 (middle panel) or perfused with PmPV2 preincubated with GlnNH<sub>2</sub> (lower panel). (C) TEM imaging of PmPV2 pore formed on liposomes. (a) POPC:Cho liposomes carrying PmPV2 pore-like structures in side view (arrowheads). 50kx amplification. Bar 100 nm. (b) Top view of ring-like structure form by PmPV2 on the liposome surface at 225kx amplification. *Inset*: 640kx amplification. Bar 20 nm.



bioRxiv preprint doi: <https://doi.org/10.1101/2019.12.23.880021>; this version posted December 23, 2019. The copyright holder for this preprint (which was not certified by peer review) is the author/funder, who has granted bioRxiv a license to display the preprint in perpetuity. It is made available under aCC-BY-ND 4.0 International license.

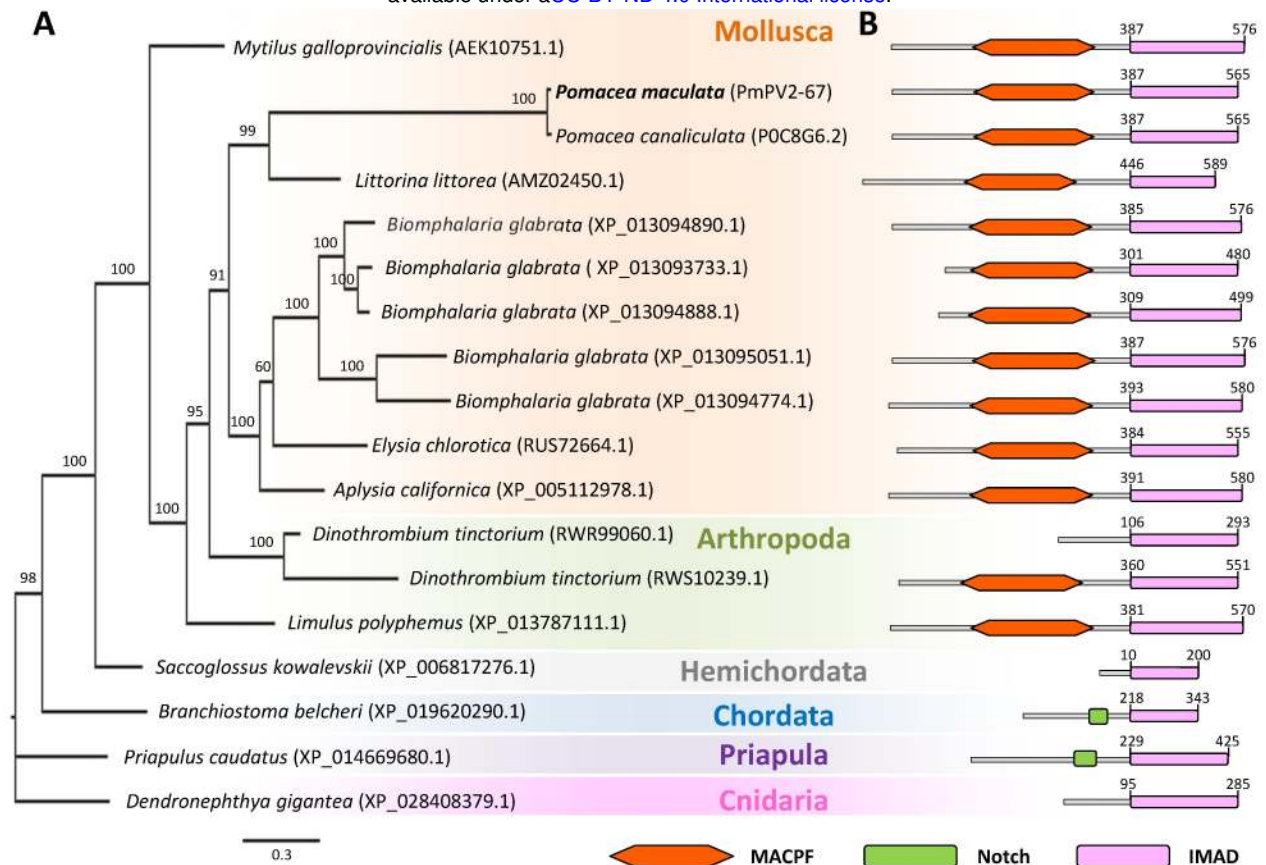


#### Figure 4. Phylogeny and occurrence of Invertebrate MACPF Accessory Domain (IMAD).

(A) Unrooted phylogenetic tree of homologous sequences of Ct-PmPV2-67. Homologues were retrieved from BLASTp analysis, sequences aligned by MUSCLE and phylogeny reconstructed using MrBayes. Node numbers represent Bayesian posterior probabilities (in percentage) of finding a given clade.

(B) Domain architecture of Ct-PmPV2-67 homologue sequences highlighting the relative position of the Nt-MACPF and Ct-IMAD domains, as found by ThreaDom and Pfam analysis.

AEK10751.1: MACPF domain containing protein (*Mytilus galloprovincialis*); POC8G6.2: Perivitellin-2 67 kDa subunit (*Pomacea canaliculata*); AMZ02450.1: Perivitellin-2 67 kDa subunit-like (*Littorina littorea*); XP\_013094890.1, XP\_013093733.1, XP\_013094888.1, XP\_013095051.1, and XP\_013094774.1: Perivitellin-2 67 kDa subunit-like (*Biomphalaria glabrata*); RUS72664.1: Hypothetical protein (*Elysia chlorotica*); XP\_005112978.1: Perivitellin-2 67 kDa subunit-like (*Aplysia californica*); RWR99060.1, and RWS10239.1: Perivitellin-2 67 kDa subunit-like (*Dinothrombium tinctorium*); XP\_013787111.1: Perivitellin-2 67 kDa subunit-like (*Limulus polyphemus*); XP\_006817276.1: Perivitellin-2 67 kDa subunit-like (*Saccoglossus kowalevskii*); XP\_019620290.1: Uncharacterized protein (*Branchiostoma belcheri*); XP\_014669680.1: Uncharacterized protein (*Priapulus caudatus*); XP\_028408379.1: Perivitellin-2 67 kDa subunit-like (*Dendronephthya gigantea*).